Inhibition of Aluminum Corrosion with the Addition of the Tris(pentafluoroethyl)trifluorophosphate Anion to a Sulfonylamide-based Ionic Liquid for Sodium-ion Batteries

Jinkwang Hwang,[*,z] Ikuma Aoyagi, Masaya Takiyama, Kazuhiko Matsumoto,[*,z] Rika Hagiwara[*]

Graduate School of Energy Science, Kyoto University, Sakyo-ku, Kyoto 606-8501, Japan
*Electrochemical Society Member.

Corresponding authors: Kazuhiko Matsumoto and Jinkwang Hwang
[z]E-mail: k-matsumoto@energy.kyoto-u.ac.jp (K.M.) and hwang.jinkwang.5c@kyoto-u.ac.jp (J.H)

This paper is invited for a focus issue of the Journal of the Electrochemical Society to be titled Nucleation and Growth: Measurements, Processes and Materials.

Abstract

Ionic liquids (ILs) based on sulfonylamide-type anions have gained widespread utility as electrolytes for secondary batteries. Although sulfonylamide-based IL electrolytes are known to form a stable passivation layer that prevents Al corrosion, the Al electrode in the [Na[FSA]-[C_2C_1im][FSA] ([FSA] = bis(fluorosulfonyl)amide and [C_2C_1im] = 1-ethyl-3-methylimidazolium) IL, is found to be afflicted by pitting corrosion at potentials above 4 V vs. Na^+/Na during electrochemical measurement at 90 °C. Therefore, this study investigates the suppressive effect of $[FAP]^-$ (FAP = tris(pentafluoroethyl)trifluorophosphate) on the Al corrosion behavior of the IL electrolyte. Here, the inhibited corrosion of the Al electrode is confirmed through a series of cyclic voltammetry measurements, scanning electron microscopy, and energy-dispersive X-ray spectroscopy. Charge-discharge tests performed using a $Na_3V_2(PO_4)_2F_3$ positive electrode demonstrates that the addition of $[FAP]^-$ into the IL enhances cycling performance at the intermediate temperature of 90 °C.

Keywords: sodium-ion batteries; electrolytes; ionic liquids; Al corrosion; current collectors; tris(pentafluoroethyl)trifluorophosphate

Introduction

Amidst the ongoing renewable energy trend, sodium-ion batteries (SIBs) are quickly emerging as auspicious energy storage devices for large-scale applications due to the natural abundance and low prices of sodium resources.[1-5] Efforts to accrue these benefits have placed electrolyte design as one of the primary platforms for optimizing SIB electrochemical performance and other metrics such as thermal stability, safety, and even commercial viability. In this context, organic electrolytes encompassing Na salts such as Na[ClO_4], Na[PF_6], and Na[FSA] (FSA = bis(fluorosulfonyl)amide), mixed with carbonate organic solvents have gained widespread utility in SIB studies on the merits of their low viscosities and high ionic conductivities.[1,6-13] Despite these expedient properties, the practical operability of carbonate-based electrolytes is limited to medium temperature ranges (< 60 °C) due to their susceptibility to fire hazards arising from thermal runaway and the formation of thermally unstable solid-electrolyte interphase (SEI) at higher temperatures.[13-15] As such, the design of advanced electrolytes with improved electrochemical and physicochemical stability is considered pivotal for SIB deployment.[6,16-20]

Electrolyte development inquests have brought focus to ionic liquids (ILs) – a class of liquid salts entirely comprised of ions – as safer electrolyte alternatives for secondary batteries and electrochemical capacitors due to their exceptional capabilities such as flame retardancy, low volatility, and high electrochemical stability.[21-24] Among the IL electrolytes explored so far, $[FSA]^-$ (**Figure 1a**)- based ILs have gained immense traction in secondary battery development studies due to their high physicochemical and electrochemical properties.[25-29] Most notably, [C_2C_1im][FSA] (C_2C_1im = 1-ethyl-3-methylimidazolium) (**Figure 1b**) has been found to manifest a large liquid-phase temperature range spanning from below 0 °C to over 100 °C, and a wide electrochemical window coupled with a relatively

high ionic conductivity (16.6 mS cm^{-1}) – exemplary properties for functional energy storage devices.[30-35] Accordingly, secondary batteries encompassing [C_2C_1im][FSA] ILs alongside *M*[FSA] salts (*M* = Li, Na, and K) have been reported to effectively sustain operations over a wide temperature range and exhibit high electrochemical performance. [26,36-41] In this light, these IL electrolytes are seen as ideal candidates for developing intermediate temperature operation batteries (~100 °C) capable of harnessing waste heat from other operations while maintaining efficient kinetic and electrochemical performance, albeit their success is also contingent on the optimization of other cell components such as electrodes.

The compatibility between an electrolyte and standard cell components such as Al current collectors is a key requisite in battery development. From this perspective, the suitability of ILs incorporating $[FSA]^-$ becomes even more apparent due to their ability to significantly inhibit Al corrosion;[13,42,43] unlike their FSA-based organic counterparts, which exhibit severe Al corrosion behavior.[44-46] In spite of this quality, a recent study (by our group) into the electrochemical performance of a $Na_3V_2(PO_4)_2F_3$ positive electrode in Na[FSA]-[C_2C_1im][FSA] IL electrolyte at elevated temperatures (90 °C) reported the occurrence of a large irreversible charge capacity that even exceeded the theoretical capacity of the positive electrode. This unforeseen irreversible capacity was attributed to the corrosion of the Al current collector, suggesting that suppression of Al corrosion in the electrolyte was inadequate at elevated temperatures. Taking this observation into account, a viable solution for suppressing the Al corrosion behavior of the Na[FSA]-[C_2C_1im][FSA] IL electrolyte can be considered to be an essential milestone towards their practical utilization in intermediate temperature SIBs.

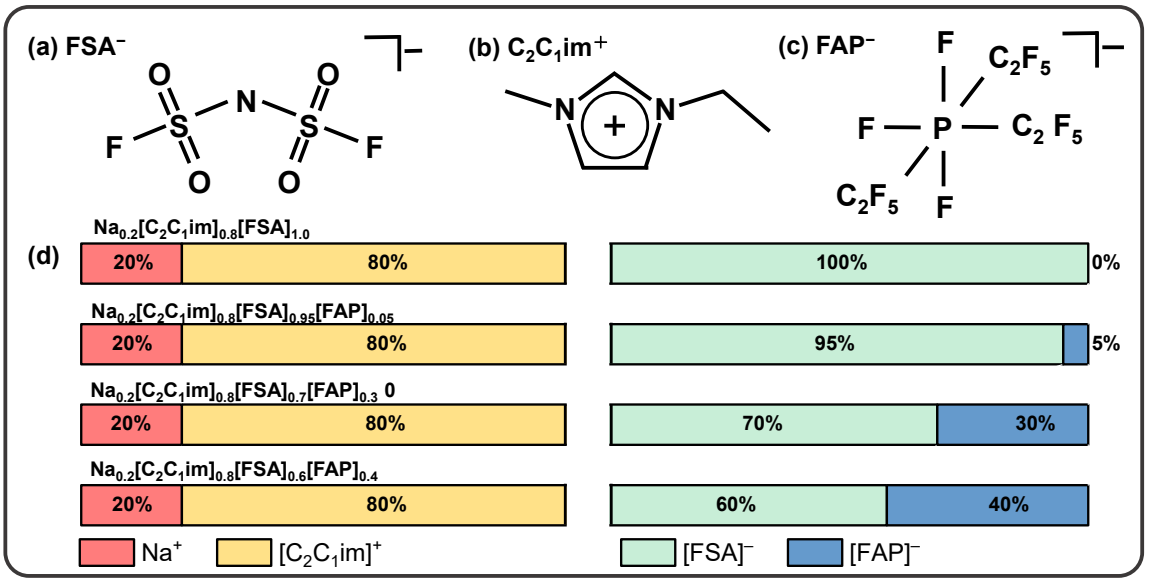

Figure 1. Structure of (a) 1-ethyl-3-methylimidazolium cation ($[C_2C_1im]^+$), (b) bis(fluorosulfonyl)amide anion ($[FSA^-]$), and (c) tris(pentafluoroethyl)trifluorophosphate anion ($[FAP^-]$). (d) Molar ratio of cations and anions in the present ILs.

Previous studies have reported electrolytes (both organic electrolytes and ILs) comprising $[FAP]^-$ (FAP = tris(pentafluoroethyl)trifluorophosphate, **Figure 1c**) to exhibit excellent anodic stability and good cycling performances with high voltage electrode materials.[47-50] As such, the use of $[FAP]^-$ as an additive for the $[FSA]^-$-based ILs can be postulated to be a prudent approach to suppressing Al corrosion during operations. Thus, in a bid to ascertain this conjecture, this study investigates the influence of a $[FAP]^-$ additive on the Al corrosion behavior and electrochemical properties (i.e., electrochemical window and charge-discharge performance with $Na_3V_2(PO_4)_2F_3$) of Na[FSA]-$[C_2C_1im][FSA]$ IL. Here, field emission scanning electron microscopy (FE-SEM), energy-dispersive X-ray spectroscopy (EDX), X-ray fluorescence (XRF) measurements, and Raman spectroscopy are employed to clarify the Al corrosion behavior (or lack thereof) of Na$[C_2C_1im][FSA]$ IL electrolytes formulated with and without $[FAP]^-$.

Experimental

Materials and electrolytes. – All samples: electrolytes, ILs, electrodes, and cells, were handled and prepared in an Ar-filled glove box (H_2O < 1 ppm and O_2 <1 ppm). Na[FSA] (Mitsubishi Materials Electronic Chemicals, purity > 99%) was dried at 100 °C under vacuum for 24 h. [C_2C_1im][FSA] (Kanto Chemicals, purity > 99.9%) and [C_2C_1im][FAP] (Sigma-Aldrich, purity ≤ 100%) were dried at 80 °C under vacuum for 24 h. The ILs used for this work were mixed in the target ratios and stirred for 24 h at room temperatures. $Na_{0.2}[C_2C_1im]_{0.8}[FSA]_{1.0}$ (Na[FSA] : [C_2C_1im][FSA] = 20 : 80 mol%), $Na_{0.2}[C_2C_1im]_{0.8}[FSA]_{0.95}[FAP]_{0.05}$ (Na[FSA] : [C_2C_1im][FSA] : [C_2C_1im][FAP] = 20 : 75 : 5 mol%), $Na_{0.2}[C_2C_1im]_{0.8}[FSA]_{0.7}[FAP]_{0.3}$ (Na[FSA] : [C_2C_1im][FSA] : [C_2C_1im][FAP] = 20 : 50 : 30 mol%), $Na_{0.2}[C_2C_1im]_{0.8}[FSA]_{0.6}[FAP]_{0.4}$ (Na[FSA] : [C_2C_1im][FSA] : [C_2C_1im][FAP] = 20 : 40 : 40 mol%, and $Na_{0.2}[C_2C_1im]_{0.8}[FSA]_{0.7}[PF_6]_{0.3}$ (Na[FSA] : [C_2C_1im][FSA] : [C_2C_1im][PF_6] = 20 : 50 : 30 mol%). A summary of the present electrolyte compositions has been furnished in **Figure 1d**.

Electrode and cell preparations. – Coin cells (2032-type) used for linear sweep voltammetry (LSV) and cyclic voltammetry (CV) were assembled using Pt and Al plates (Nilaco Corporation) as the working electrodes (10 mm in diameter). Sodium metal (Aldrich purity > 99.95%) stretched into foil was affixed onto the Al plate and used as the counter electrode (13 mm in diameter). In line with a previous report, the carbon-coated $Na_3V_2(PO_4)_2F_3$ (NVPF) composite was synthesized via a two-step process.[13] First, the carbon-coated VPO_4 (VPO_4-C) precursor was prepared through the sol-gel method. The prepared VPO_4/C was then mixed with NaF (2:3 molar ratio) and ball-milled for 1 h before heating at 700 °C for 8 h under an Ar atmosphere. Combustion analysis determined the final NVPF composite to have a carbon

content of 12wt%. A slurry comprising the NVPF mixed with acetylene black and PVDF (80:15:5) in *N*-methylpyrrolidone was pasted on an Al foil to prepare the positive electrode. The electrodes were dried under vacuum at 353 K for 12 h. The active materials of the positive electrode were packed with a loading mass of approximately 1 mg-active material cm^{-2} after the drying process. A glass microfiber (Whatman, GF/A; 16 mm in diameter and 260 μm in thickness) immersed in the as-prepared electrolyte was used as a separator.

Analysis. – All the electrochemical measurements were performed in a temperature-controlled thermostatic chamber (SU-242, ESPEC) at 25 and 90 °C. CV and LSV tests were conducted at 1 mV s^{-1} (Bio-Logic VSP potentiostat) to evaluate electrochemical stability. The potentials of Pt and Al electrodes were swept from the rest potential to 5.5 V vs. Na^+/Na and to 6.0 V vs. Na^+/Na, respectively, to determine the anodic stability. The potential of the Al electrode was swept from the rest potential to –0.2 V to evaluate Na metal deposition/dissolution properties. After CV tests, the Al electrodes were washed with dimethyl carbonate (DMC, Fujifilm Wako, purity > 98.0%) and dried at 60°C for 1 h under vacuum. The surface of the Al electrodes were thereafter analyzed by field emission-scanning electron microscopy, Hitachi SU-8020) and EDX (Horiba EMAXEvolution X-max). The charge-discharge properties were tested using a charge-discharge unit (HJ1001SD8, Hokuto Denko Corp.). A constant current of 1C (1C = 128 mA g^{-1}) and cutoff voltages of 2.0–4.3 V were set to the charge-discharge and cycling tests. A Raman instrument (DXR3, Thermo Scientific) was used to record the Raman spectra of ILs using the diode-pumped solid-state laser with an excitation wavelength of 532 nm. After the CV tests, the coin cells were disassembled and their entire contents immersed in propylene carbonate (5 cm^3) for one day to extract all the Al species in the electrolyte. Subsequently, the presence of Al species in the

electrolyte after CV tests was ascertained through X-ray fluorescence (XRF) spectroscopy (EDXL 300 Rigaku Corporation) under a helium atmosphere.

Results and Discussion

Electrochemical Stability of ILs

In an effort to determine the anodic and cathodic stabilities of Na[FSA]-[C_2C_1im][FSA] IL electrolytes with and without the $[FAP]^-$ additive at ambient- and elevated temperatures, cyclic voltammetry (CV) and linear sweep voltammetry (LSV) measurements were performed on Al and Pt working electrodes, respectively, alongside electrolytes adopting the $Na_{0.2}[C_2C_1im]_{0.8}[FSA]_{1.0}$ and $Na_{0.2}[C_2C_1im]_{0.8}[FSA]_{0.7}[FAP]_{0.3}$ compositions and the Na counter electrode at 25 and 90 °C. To discern the influence of the $[FAP]^-$ anion in the [FSA]-IL, an electrolyte sample comprising a different Na[FSA] concentration ($Na_{0.3}[C_2C_1im]_{0.7}[FSA]_{1.0}$) and another incorporating a $[PF_6]^-$ anion ($Na_{0.2}[C_2C_1im]_{0.8}[FSA]_{0.7}[PF_6]_{0.3}$) were also prepared and subjected to measurements under the same conditions for comparison.

The CV curves obtained from the low potential region (from the rest potential to −0.2 V) of the Al working electrode operated in the $Na_{0.2}[C_2C_1im]_{0.8}[FSA]_{1.0}$ and $Na_{0.2}[C_2C_1im]_{0.8}[FSA]_{0.7}[FAP]_{0.3}$ ILs at 25 and 90 °C are shown in **Figure 2**. Here, sodium metal deposition/dissolution on the Al electrode was observed to occur around 0 V vs. Na^+/Na during the successive cathodic and anodic scans, respectively, at both temperatures. Irrespective of the presence of $[FAP]^-$, Na metal deposition at 25 °C is noted to occur with a deposition overpotential of about 0.1 V. Likewise, the addition of $[FAP]^-$ is also seen to have no significant influence on the Coulombic efficiencies of Na deposition/dissolution at both temperatures (slightly inferior to without $[FAP]^-$). Even so, both ILs exhibited dramatic

improvements in their dissolution/deposition efficiency: from 25-38% (25 °C) to 80-85% (90 °C) and a decrease in overpotential upon temperature elevation. As such, these results augur the possibility of highly efficient Na metal batteries capable of facilitating elevated temperatures with the aid of IL electrolytes.

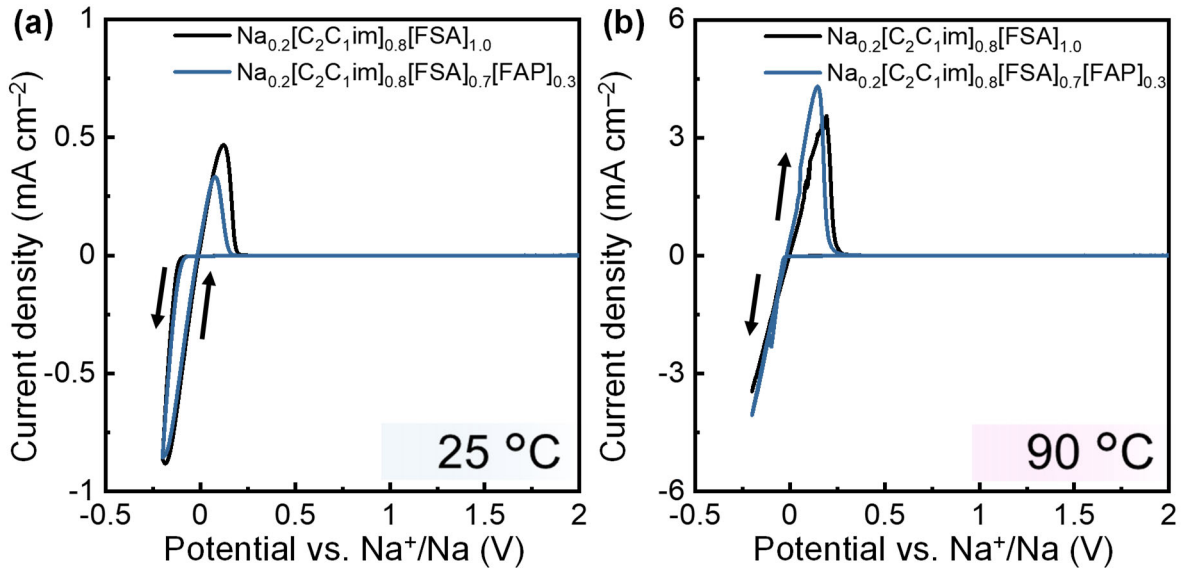

Figure 2. Cyclic voltammograms of an Al electrode in the $Na_{0.2}[C_2C_1im]_{0.8}[FSA]_{1.0}$ and $Na_{0.2}[C_2C_1im]_{0.8}[FSA]_{0.7}[FAP]_{0.3}$ ILs scanned from the rest potential to −0.2 V at (a) 25 °C and (b) 90 °C. Scan rate: 1 mV s^{-1}.

To shed more light on the anodic stabilities of the $Na_{0.2}[C_2C_1im]_{0.8}[FSA]_{1.0}$ and $Na_{0.2}[C_2C_1im]_{0.8}[FSA]_{0.7}[FAP]_{0.3}$ IL electrolytes, LSV measurements were conducted using a Pt working electrode, as shown in **Figures 3a, b**. During measurements at 25 °C (**Figure 3a**), the oxidation current was noted to rise from 5.1 V for both electrolytes. Further measurements at 90 °C showed the oxidation current to commence at a slightly lower voltage of 4.8 V in both the cases (**Figure 3b**). It is worth noting that the comparative test performed using the $Na_{0.2}[C_2C_1im]_{0.8}[FSA]_{0.7}[PF_6]_{0.3}$ IL also yielded similar anodic limits (see **Figure S1**, Supplementary Materials), suggesting that the anodic limits of the present electrolytes

were mainly engendered by the irreversible decomposition.[51] Therefore, the addition of $[FAP]^-$ and $[PF_6]^-$ does not improve the anodic stability intrinsic to the Na[FSA]-$[C_2C_1im][FSA]$ IL.

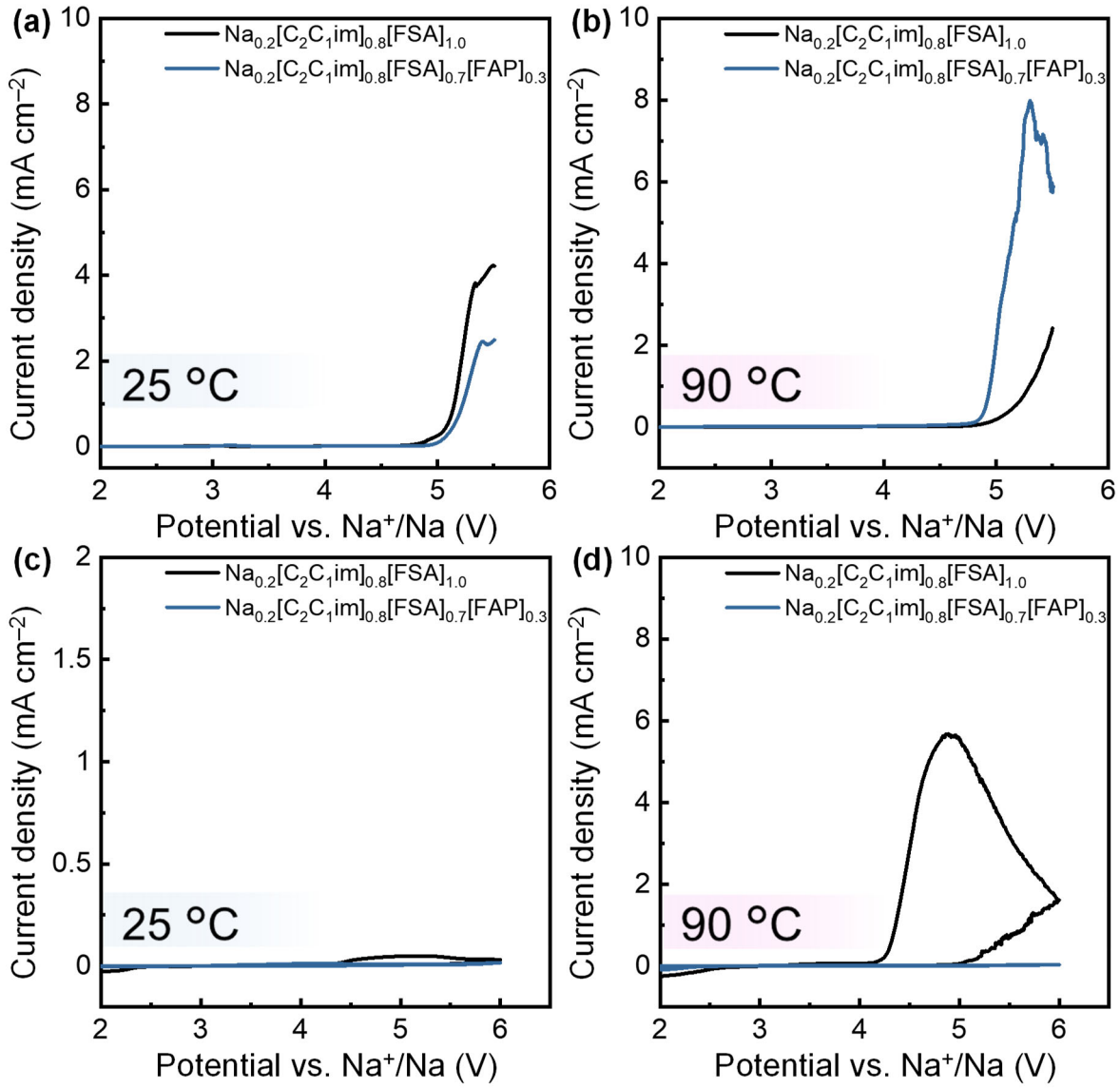

Figure 3. Linear sweep voltammograms of the Pt electrode in the $Na_{0.2}[C_2C_1im]_{0.8}[FSA]_{1.0}$ and $Na_{0.2}[C_2C_1im]_{0.8}[FSA]_{0.7}[FAP]_{0.3}$ ILs scanned from the rest potential to 5.5 V at (a) 25 °C and (b) 90 °C. Scan rate: 1 mV s^{-1}. Cyclic voltammograms of the Al electrode in the $Na_{0.2}[C_2C_1im]_{0.8}[FSA]_{1.0}$, and $Na_{0.2}[C_2C_1im]_{0.8}[FSA]_{0.7}[FAP]_{0.3}$ ILs scanned from the rest potential to 6 V at (c) 25 °C and (d) 90 °C. Scan rate: 1 mV s^{-1}.

The Al corrosion behavior was further scrutinized through CV measurements

conducted on the Al working electrode in the $Na_{0.2}[C_2C_1im]_{0.8}[FSA]_{1.0}$ and $Na_{0.2}[C_2C_1im]_{0.8}[FSA]_{0.7}[FAP]_{0.3}$ ILs (**Figure 3c, d**). Here, the curves obtained from the $Na_{0.2}[C_2C_1im]_{0.8}[FSA]_{1.0}$ IL show the anodic current above 4V at 25 and 90 °C typical potentials for Al corrosion in electrolytes comprising the sulfonylamide-type anion. However, no current flow was visualized, even during scans at 6.0 V, during measurements using the $Na_{0.2}[C_2C_1im]_{0.8}[FSA]_{0.7}[FAP]_{0.3}$ IL electrolyte at both temperatures; an indication that the addition of $[FAP]^-$ improved the passivation stability of the Al electrode thereby mitigating corrosion. To further validate these results, CV measurements were performed on the IL with a higher Na[FSA] molar fraction ($Na_{0.3}[C_2C_1im]_{0.7}[FSA]_{1.0}$) and the IL with $[PF_6]^-$ ($Na_{0.2}[C_2C_1im]_{0.8}[FSA]_{0.7}[PF_6]_{0.3}$) at 25 and 90 °C (**Figure S2**, Supplementary Materials). The IL with a higher Na[FSA] molar ratio demonstrated Al corrosion behavior at both the temperatures with marked exacerbation at 90 °C. This observation clearly connotes that increasing the Na concentration does not effectively suppress the Al corrosion. However, the IL with $[PF_6]^-$ displayed suppressed Al corrosion at 25 °C (**Figure S3**, Supplemental Materials), the result is congruent with previous studies which have demonstrated the $[PF_6]^-$ to be effective in suppressing Al corrosion in lithium-ion batteries at high potential regions[42] although it was not as effective as $[FAP]^-$ during scans performed at 90 °C. The difference in the effect of suppressing Al corrosion between $[FAP]^-$ and $[PF_6]^-$ is considered to be related to the perfluoroethyl group (CF_2CF_3) in $[FAP]^-$. As three fluorine atoms are replaced by three CF_2CF_3 group, it provides different components of the Al passivation layer. Another possible reason is the lower donor number of $[FAP]^-$,[52] which decreases the solubility of Al species into the ionic liquid.

Pitting Corrosion Behavior of Al Current Collector

The CV measurements clearly highlight that the addition of $[FAP]^-$ is effective in

mitigating Al corrosion in electrolytes containing $[FSA]^-$, especially at 90 °C. To gain insight into the nature of Al corrosion behavior in the $Na_{0.2}[C_2C_1im]_{0.8}[FSA]_{1.0}$ IL electrolyte, the surface morphology and elemental distribution of the Al electrode obtained after CV scans at 90 °C (**Figure 3d**) were examined through FE-SEM and EDX analyses. As shown by the SEM images in **Figure 4**, the Al electrode surface is marked by severe pitting corrosion, in line with the observations from the previous measurements. Additionally, EDX-mapping indicates the presence of N, F, O, and S elements on the electrode surface, further corroborating that the corrosion process involved $[FSA]^-$ decomposition.[13]

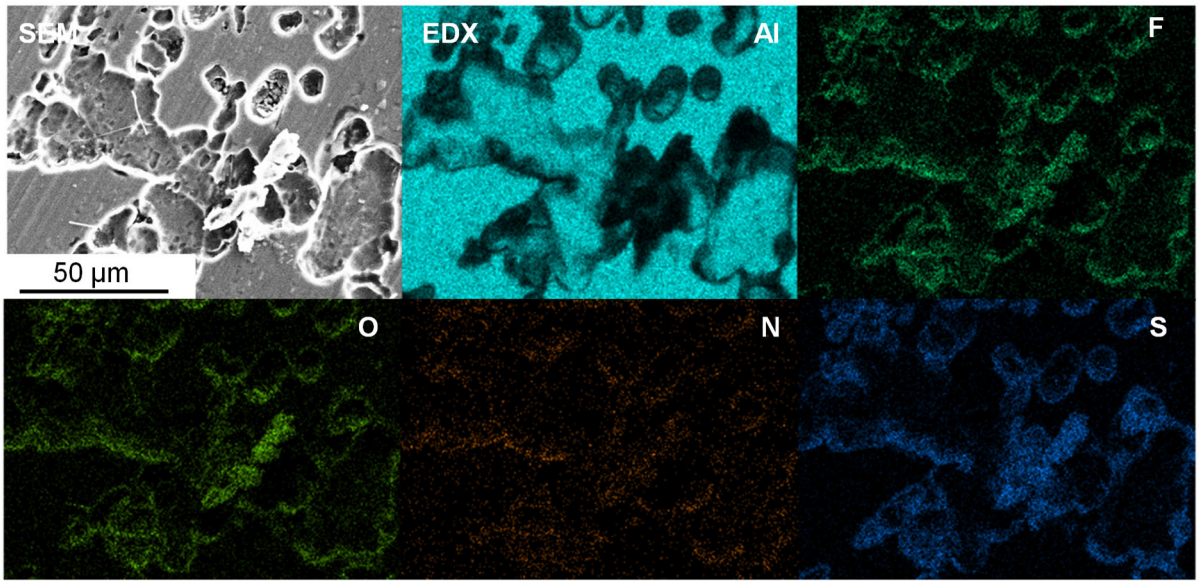

Figure 4. FE-SEM and EDX mapping images of the Al electrode after the CV test (in **Figure 3d**) in $Na_{0.2}[C_2C_1im]_{0.8}[FSA]_{1.0}$ at 90 °C. The EDX mapping corresponds to the SEM images at the top left. The elemental compositions of the Al electrode are observed to be Al: 66. 4wt%, F: 4.9 wt%, O: 6.9 wt%, N: 3.6 wt%, S: 4.2 wt% and Na 1.2 wt%

To ascertain the nature of Al corrosion upon the addition of $[FAP]^-$, the SEM and EDX-mapping images of the Al electrode were scanned in the $Na_{0.2}[C_2C_1im]_{0.8}[FSA]_{0.7}[FAP]_{0.3}$ IL at 90 °C (**Figure 3d**) are furnished in **Figure 5**. Unlike the electrode in $Na_{0.2}[C_2C_1im]_{0.8}[FSA]_{1.0}$ IL electrolyte, the SEM images in **Figure 5** display

no pitting corrosion on the electrode surface. At high magnification, deposits with diameters in the ~5–20 nm range are seen to be homogenously distributed across the electrode surface. EDX analyses confirm these deposits to be decomposition products of the $[FAP]^-$ and $[FSA]^-$ components from the electrolyte. Although the deposits can be posited to work as a stable passivation layer that prevents pitting corrosion on the Al current collector, the other part is also supposed to be covered with the decomposition products. The suppressed Al corrosion in the IL with $[FAP]^-$ is further validated through XRF analysis performed on the IL electrolytes after the CV tests. The data reveals lower Al concentrations (234 ppm) in the IL with $[FAP]^-$ in comparison to its counterpart without $[FAP]^-$ (1970 ppm).

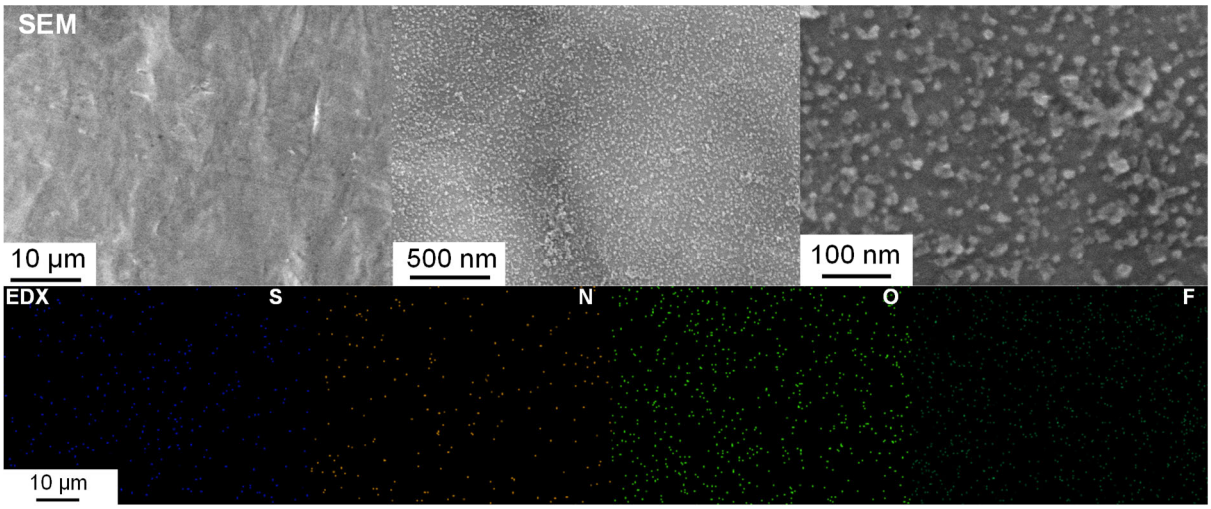

Figure 5. FE-SEM and EDX mapping images of the Al electrode after the CV test (**Figure 3d**) in the $Na_{0.2}[C_2C_1im]_{0.8}[FSA]_{0.7}[FAP]_{0.3}$ IL at 90 °C. The EDX mapping corresponds to the SEM images at the top left. The elemental compositions of the Al electrode are observed to be Al: 90.9 wt%, F: 1.6 wt%, O: 3.3 wt%, N: 1.6 wt%, S: 1.6 wt% and Na 0.5 wt%

Considering that free $[FSA]^-$ (along with other sulfonylamide anions: (fluorosulfonyl)(trifluoromethylslufonyl)amide (FTA) and bis(trifluoromethylsulfonyl)amide TFSA) is known to accelerate Al corrosion,[42,53-55] the coordination states of $[FSA]^-$ are expected to provide essential insight into the Al corrosion behavior in the present IL electrolytes. Therefore, IL electrolytes with varying ratios of $[FSA]^-$ and $[FAP]^-$ were

subjected to Raman spectroscopy, as shown in **Figure 6**. The wide range spectra (200 to1500 cm^{-1}) are shown in **Figure 6a**. The representative vibrational modes of $[FSA]^-$ in the 700–800 cm^{-1} and 1180–1260 cm^{-1} spectral ranges are provided in **Figure 6b and 6c**, respectively. In the neat $[C_2C_1im][FSA]$ IL spectrum, the peaks emerging at 726 and 1216 cm^{-1} are attributed to the S–N–S bending mode and S=O stretching modes of the weakly bound $[FSA]^-$ (free $[FSA]^-$).[56-59] In the case of the spectra from ILs comprising $[FAP]^-$, the strong peak at 743 cm^{-1} is assigned to the F–C–F deformation mode of $[FAP]^-$.[60,61]Although free $[FSA]^-$ was still observed at this composition (up to 40 mol %) according to a previous report,[57] the blue-shifts observed in the $[FSA]^-$ peaks (from 724 to 743 cm^{-1} and from 1216 to 1225 cm^{-1}) result from the increased concentration of Na which suggests the presence of a stronger association between $[FSA]^-$ and Na^+ $((Na[FSA]_n)^{1-n}$. Notably, the addition of $[FAP]^-$ also induces blue-shifts because Na^+ preferentially coordinates to $[FSA]^-$ as a result of the higher basicity of $[FSA]^-$ in comparison to $[FAP]^-$. By this token, the resulting $Na^+/[FSA]^-$ ratio increases with higher amounts of $[FAP]^-$.

The electrochemical, optical observations and Raman spectra reported in the present study evince that the suppression of Al corrosion in the presence of $[FAP]^-$ cumulatively results from the following factors: i) the concentration of the free $[FSA]^-$ abrading the oxide layer (passivation layer) of the Al current collector is reduced upon addition of $[FAP]^-$; ii) Al species have lower solubilities in the ILs with $[FAP]^-$; iii) the electrolyte decomposition products from the IL with $[FAP]^-$ form a stable passivation layer on the Al current collector surface.

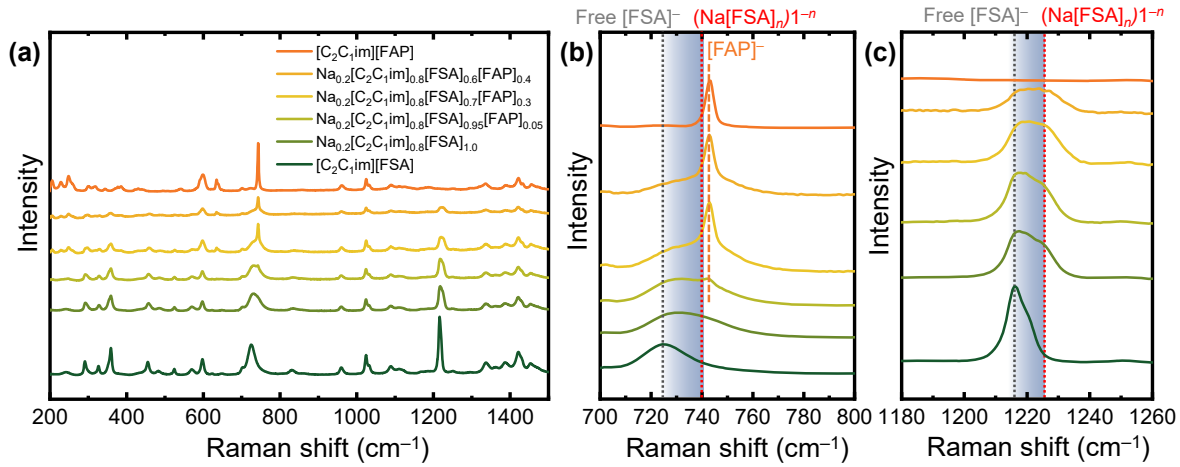

Figure 6. Raman spectra of ILs with varying ratios of $[FSA]^-$ and $[FAP]^-$ in the range of (a) 200-1500 cm^{-1}, (b) 700-800 cm^{-1}, and (b) 1180-1260 cm^{-1}.

Charge-discharge Performance

The effect of $[FAP]^-$ (and consequently suppressed Al corrosion) on the electrochemical behavior of $Na_3V_2(PO_4)_2F_3$ positive electrode in the present IL electrolytes was examined through charge-discharge tests at 25 and 90 °C. This electrode material is known to yield two-step redox plateaus at the high potentials of 3.7 and 4.2 V vs. Na^+/Na and was thus deemed to be apposite for the present investigation.[62-67] Room temperature measurements (25 °C) of the $Na_3V_2(PO_4)_2F_3$ in the $Na_{0.2}[C_2C_1im]_{0.8}[FSA]_{1.0}$ and $Na_{0.2}[C_2C_1im]_{0.8}[FSA]_{0.7}[FAP]_{0.3}$ IL electrolytes 1C = 128 mA g^{-1} are shown by the charge-discharge curves in **Figure S4**. Here, both the electrolytes are noted to yield comparable first cycle discharge capacities (95 mAh g^{-1}). However, the $Na_{0.2}[C_2C_1im]_{0.8}[FSA]_{0.7}[FAP]_{0.3}$ IL shows slightly better cycleability, delivering capacity retention of 91% after 100 cycles (**Figure S5**). The charge-discharge curves obtained at 90 °C are provided in **Figure 7**. At elevated temperatures, both the electrolytes show significant improvements in their initial cycle discharge capacities (118 mAh g^{-1} at 1C) compared with the measurements at 25 °C. The higher capacities are attributed to the enhanced electrode kinetics and improved ion transport upon temperature elevation. Even so, the $Na_{0.2}[C_2C_1im]_{0.8}[FSA]_{1.0}$ IL exhibits

severe irreversible capacity, delivering an initial cycle Coulombic efficiency of 66%. Furthermore, the IL without $[FAP]^-$ is afflicted with increasing polarization and fluctuant charge-discharge curves, thereby producing remarkably low Coulombic efficiency throughout the measurement (**Figure 7**a and **7c**) (capacity: 51.1 mAh g^{-1} and Coulombic efficiency: 51% at the 30th cycle). This deterioration is ascribed to the oxidative decomposition of the electrolyte coupled with Al corrosion behavior in the IL without $[FAP]^-$. On the other hand, the $Na_{0.2}[C_2C_1im]_{0.8}[FSA]_{0.7}[FAP]_{0.3}$ IL electrolyte displays significantly improved cycle stability (**Figure 7**b,d), yielding a capacity of 108.3 mAh g^{-1} and a Coulombic efficiency of 95% at the 30th cycle. These electrochemical results suggest that the suppressed Al corrosion in the IL containing $[FAP]^-$ significantly contributes to the high cycle performance of the $Na_3V_2(PO_4)_2F_3$ electrode.

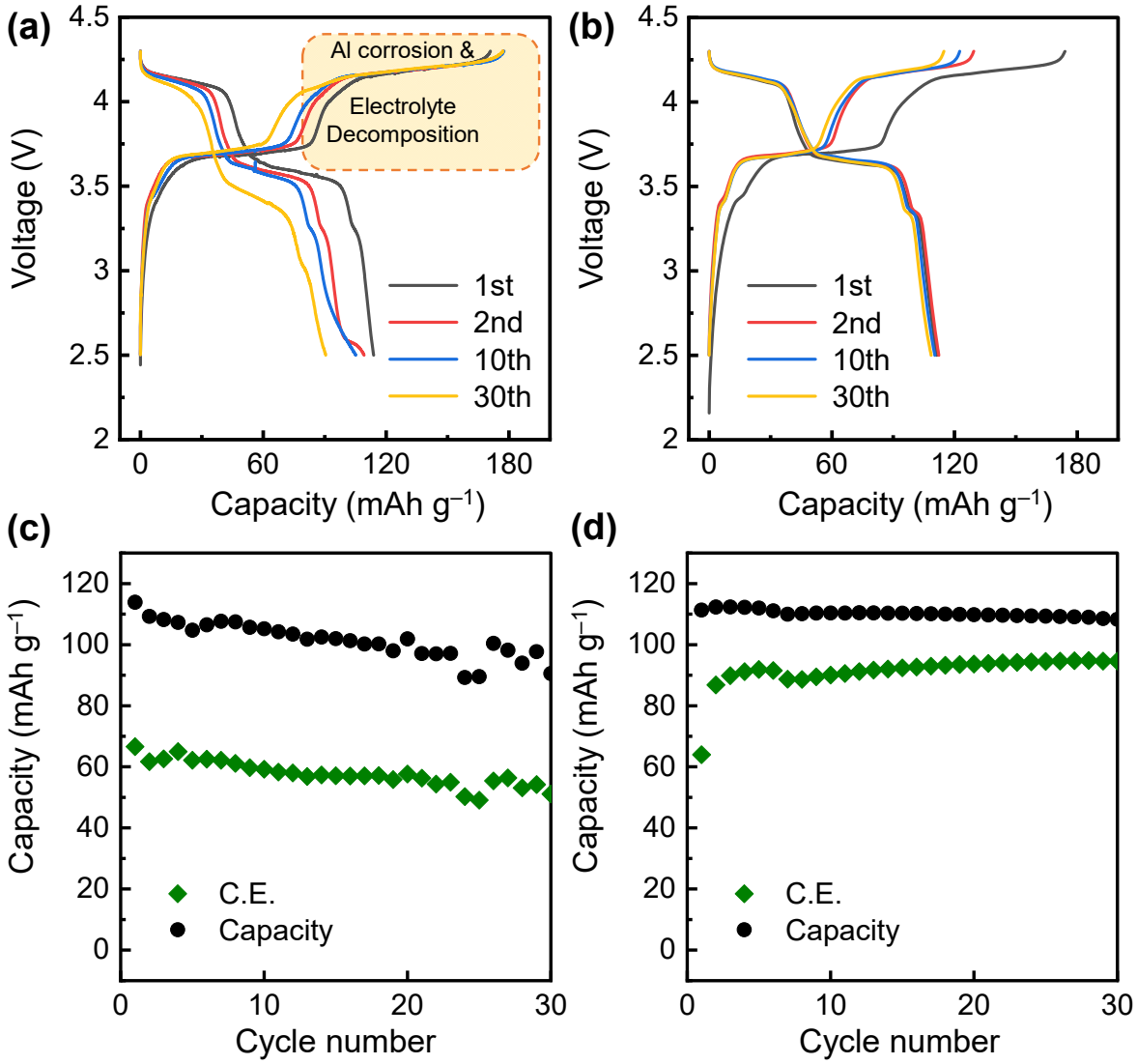

Figure 7. Galvanostatic charge-discharge curve of (a) the Na/$Na_{0.2}[C_2C_1im]_{0.8}[FSA]_{1.0}$/$Na_3V_2(PO_4)_2F_3$ cell and (b) the Na/$Na_{0.2}[C_2C_1im]_{0.8}[FSA]_{0.7}[FAP]_{0.3}$/$Na_3V_2(PO_4)_2F_3$ cell and (c, d) their corresponding cycle performances at 90 °C. Cutoff range: 2.5–4.3 V. Charge-discharge rate: 1C.

Conclusions

This study reports the inhibitory effect of $[FAP]^-$ on Al corrosion in the Na[FSA]-$[C_2C_1im][FSA]$ IL at 25 and 90°C. The results indicated that the Na[FSA]-$[C_2C_1im][FSA]$ IL moderately suppressed Al corrosion at 25°C, whereas elevated temperature (90°C) operations at potentials above 4 V vs. Na^+/Na caused severe pitting corrosion on the Al electrode.

However, the addition of $[FAP]^-$ into the Na[FSA]-$[C_2C_1im][FSA]$ IL was seen to suppress Al corrosion even though it did not improve anodic stability with a Pt electrode. FE-SEM and EDX analyses performed after CV measurements revealed that Al corrosion was mitigated by a passivation layer formed by homogeneously distributed deposits comprising $[FSA]^-$ and $[FAP]^-$ decomposition products. Further, Raman spectroscopy demonstrated that the amount of free $[FSA]^-$ upon the addition of $[FAP]^-$ thereby diminishing Al dissolution in the Na$[C_2C_1im][FSA][FAP]$ IL as was confirmed by XRF. Finally, charge-discharge tests performed using a $Na_3V_2(PO_4)_2F_3$ electrode verified that the inhibited Al corrosion upon the addition of $[FAP]^-$ improved the electrochemical performance of the IL electrolyte, especially at elevated temperatures. These results clearly demonstrate the addition of $[FAP]^-$ to be an effective strategy for optimizing the performance of high-voltage positive electrodes in a sulfonylamide-based ILs at both room and intermediate temperatures.

Acknowledgments

This study was supported by JSPS KAKENHI Grant Number JP21H02047.

ORCID

Jinkwang Hwang: 0000-0003-4800-3158

Kazuhiko Matsumoto: 0000-0002-0770-9210

Rika Hagiwara: 0000-0002-7234-3980

References

1. N. Yabuuchi, K. Kubota, M. Dahbi, S. Komaba, *Chem. Rev.,* **114**, 11636 (2014).

2. S.-W. Kim, D.-H. Seo, X. Ma, G. Ceder, K. Kang, *Adv. Energy Mater.,* **2**, 710 (2012).

3. J.-M. Tarascon, *Nat. Chem.,* **2**, 510 (2010).

4. M. D. Slater, D. Kim, E. Lee, C. S. Johnson, *Adv. Funct. Mater.,* **23**, 947 (2013).

5. H. S. Hirsh, Y. Li, D. H. S. Tan, M. Zhang, E. Zhao, Y. S. Meng, *Adv. Energy Mater.,* **10**, 2001274 (2020).

6. A. Ponrouch, D. Monti, A. Boschin, B. Steen, P. Johansson, M. R. Palacín, *J. Mater. Chem. A,* **3**, 22 (2015).

7. A. Ponrouch, E. Marchante, M. Courty, J.-M. Tarascon, M. R. Palacín, *Energy Environ. Sci.,* **5**, 8572 (2012).

8. G. Åvall, J. Mindemark, D. Brandell, P. Johansson, *Adv. Energy Mater.,* **8**, 1703036 (2018).

9. T. Minato, H. Kawaura, M. Hirayama, S. Taminato, K. Suzuki, N. L. Yamada, H. Sugaya, K. Yamamoto, K. Nakanishi, Y. Orikasa, H. Tanida, R. Kanno, H. Arai, Y. Uchimoto, Z. Ogumi, *J. Phys. Chem. C,* **120**, 20082 (2016).

10. D. Takamatsu, Y. Orikasa, S. Mori, T. Nakatsutsumi, K. Yamamoto, Y. Koyama, T. Minato, T. Hirano, H. Tanida, H. Arai, Y. Uchimoto, Z. Ogumi, *J. Phys. Chem. C,* **119**, 9791 (2015).

11. B. L. Ellis, L. F. Nazar, *Curr. Opin. Solid State Mater. Sci.,* **16**, 168 (2012).

12. V. Palomares, M. Casas-Cabanas, E. Castillo-Martinez, M. H. Han, T. Rojo, *Energy Environ. Sci.,* **6**, 2312 (2013).

13. J. Hwang, K. Matsumoto, R. Hagiwara, *Adv. Energy Mater.,* **10**, 2001880 (2020).

14. X. Feng, M. Ouyang, X. Liu, L. Lu, Y. Xia, X. He, *Energy Storage Mater.,* **10**, 246 (2018).

15. H. Yang, H. Bang, K. Amine, J. Prakash, *J. Electrochem. Soc.,* **152**, A73 (2005).

16. G. Yan, D. Alves-Dalla-Corte, W. Yin, N. Madern, G. Gachot, J.-M. Tarascon, *J. Electrochem. Soc.,* **165**, A1222 (2018).

17. G. A. Giffin, *J. Mater. Chem. A,* **4**, 13378 (2016).

18. H. Che, S. Chen, Y. Xie, H. Wang, K. Amine, X.-Z. Liao, Z.-F. Ma, *Energy Environ. Sci.,* **10**, 1075 (2017).

19. G. C. Yan, K. Reeves, D. Foix, Z. J. Li, C. Cometto, S. Mariyappan, M. Salanne, J. M. Tarascon, *Adv. Energy Mater.,* **9**, 1901431 (2019).
20. H. S. Hirsh, B. Sayahpour, A. Shen, W. Li, B. Lu, E. Zhao, M. Zhang, Y. S. Meng, *Energy Storage Mater.,* **42**, 78 (2021).
21. A. S. Best, A. I. Bhatt, A. F. Hollenkamp, *J. Electrochem. Soc.,* **157**, A903 (2010).
22. N. Salem, L. Nicodemou, Y. Abu-Lebdeh, I. J. Davidson, *J. Electrochem. Soc.,* **159**, A172 (2012).
23. M. P. S. Mousavi, B. E. Wilson, S. Kashefolgheta, E. L. Anderson, S. He, P. Bühlmann, A. Stein, *ACS Appl. Mater. Interfaces,* **8**, 3396 (2016).
24. T. Yamamoto, S. Nishijima, T. Nohira, *J. Phys. Chem. C,* **124**, 8380 (2020).
25. A. Fukunaga, T. Nohira, Y. Kozawa, R. Hagiwara, S. Sakai, K. Nitta, S. Inazawa, *J. Power Sources,* **209**, 52 (2012).
26. K. Matsumoto, J. Hwang, S. Kaushik, C.-Y. Chen, R. Hagiwara, *Energy Environ. Sci.,* **12**, 3247 (2019).
27. J. Hwang, K. Matsumoto, C.-Y. Chen, R. Hagiwara, *Energy Environ. Sci.,* **14**, 5834 (2021).
28. Q. Zhou, W. A. Henderson, G. B. Appetecchi, M. Montanino, S. Passerini, *J. Phys. Chem. B,* **112**, 13577 (2008).
29. Y. Zheng, D. Wang, S. Kaushik, S. Zhang, T. Wada, J. Hwang, K. Matsumoto, R. Hagiwara, *EnergyChem*, 100075 (2022).
30. K. Matsumoto, E. Nishiwaki, T. Hosokawa, S. Tawa, T. Nohira, R. Hagiwara, *J. Phys. Chem. C,* **121**, 9209 (2017).
31. T. Hosokawa, K. Matsumoto, T. Nohira, R. Hagiwara, A. Fukunaga, S. Sakai, K. Nitta, *J. Phys. Chem. C,* **120**, 9628 (2016).
32. K. Fujii, S. Seki, S. Fukuda, R. Kanzaki, T. Takamuku, Y. Umebayashi, S. Ishiguro, *J. Phys. Chem. B,* **111**, 12829 (2007).
33. K. Matsumoto, T. Hosokawa, T. Nohira, R. Hagiwara, A. Fukunaga, K. Numata, E. Itani, S. Sakai, K. Nitta, S. Inazawa, *J. Power Sources,* **265**, 36 (2014).
34. H. Matsumoto, H. Sakaebe, K. Tatsumi, M. Kikuta, E. Ishiko, M. Kono, *J. Power Sources,* **160**, 1308 (2006).
35. M. Ishikawa, T. Sugimoto, M. Kikuta, E. Ishiko, M. Kono, *J. Power Sources,* **162**, 658 (2006).

36. A. Basile, M. Hilder, F. Makhlooghiazad, C. Pozo-Gonzalo, D. R. MacFarlane, P. C. Howlett, M. Forsyth, *Adv. Energy Mater.,* **8**, 1703491 (2018).
37. J. Hwang, K. Matsumoto, T. Nohira, R. Hagiwara, *Electrochemistry,* **85**, 675 (2017).
38. J. Hwang, H. Okada, R. Haraguchi, S. Tawa, K. Matsumoto, R. Hagiwara, *J. Power Sources,* **453**, 227911 (2020).
39. J. Hwang, K. Matsumoto, R. Hagiwara, *ACS Appl. Energy Mater.,* **2**, 2818 (2019).
40. J. Hwang, K. Matsumoto, R. Hagiwara, S.-Y. Liu, J.-Y. Shin, *Small Methods,* **6**, 2101181 (2022).
41. T. Yamamoto, R. Matsubara, T. Nohira, *J. Chem. Eng. Data,* **66**, 1081 (2021).
42. E. Cho, J. Mun, O. B. Chae, O. M. Kwon, H.-T. Kim, J. H. Ryu, Y. G. Kim, S. M. Oh, *Electrochem. Commun.,* **22**, 1 (2012).
43. Q. Liu, T. L. Dzwiniel, K. Z. Pupek, Z. Zhang, *J. Electrochem. Soc.,* **166**, A3959 (2019).
44. G. G. Eshetu, S. Grugeon, H. Kim, S. Jeong, L. Wu, G. Gachot, S. Laruelle, M. Armand, S. Passerini, *ChemSusChem,* **9**, 462 (2016).
45. J. Hwang, K. Matsumoto, R. Hagiwara, *Adv. Sustainable Syst.,* **2**, 1700171 (2018).
46. L. Otaegui, E. Goikolea, F. Aguesse, M. Armand, T. Rojo, G. Singh, *J. Power Sources,* **297**, 168 (2015).
47. M. Schmidt, U. Heider, A. Kuehner, R. Oesten, M. Jungnitz, N. Ignat'ev, P. Sartori, *J. Power Sources,* **97-98**, 557 (2001).
48. D. Aurbach, *J. Power Sources,* **119-121**, 497 (2003).
49. J. S. Gnanaraj, M. D. Levi, Y. Gofer, D. Aurbach, M. Schmidt, *J. Electrochem. Soc.,* **150**, A445 (2003).
50. S. Seki, N. Serizawa, K. Hayamizu, S. Tsuzuki, Y. Umebayashi, K. Takei, H. Miyashiro, *J. Electrochem. Soc.,* **159**, A967 (2012).
51. S. P. Ong, O. Andreussi, Y. Wu, N. Marzari, G. Ceder, *Chem. Mater.,* **23**, 2979 (2011).
52. M. Schmeisser, P. Illner, R. Puchta, A. Zahl, R. van Eldik, *Eur. J. Chem.* **18**, 10969 (2012).
53. M. Morita, T. Shibata, N. Yoshimoto, M. Ishikawa, *Electrochim. Acta,* **47**, 2787 (2002).
54. L. J. Krause, W. Lamanna, J. Summerfield, M. Engle, G. Korba, R. Loch, R. Atanasoski, *J. Power Sources,* **68**, 320 (1997).
55. R.-S. Kühnel, J. Reiter, S. Jeong, S. Passerini, A. Balducci, *Electrochem. Commun.,* **38**, 117 (2014).

56. K. Fujii, H. Hamano, H. Doi, X. Song, S. Tsuzuki, K. Hayamizu, S. Seki, Y. Kameda, K. Dokko, M. Watanabe, Y. Umebayashi, *J. Phys. Chem. C,* **117**, 19314 (2013).
57. C.-Y. Chen, T. Kiko, T. Hosokawa, K. Matsumoto, T. Nohira, R. Hagiwara, *J. Power Sources,* **332**, 51 (2016).
58. K. Matsumoto, T. Oka, T. Nohira, R. Hagiwara, *Inorg. Chem.,* **52**, 568 (2013).
59. P. Shi, H. Zheng, X. Liang, Y. Sun, S. Cheng, C. Chen, H. Xiang, *Chem. Commun.,* **54**, 4453 (2018).
60. N. Borisenko, A. Lahiri, G. Pulletikurthi, T. Cui, T. Carstens, J. Zahlbach, R. Atkin, F. Endres, *Faraday Discuss.,* **206**, 459 (2018).
61. I. V. Voroshylova, F. Teixeira, R. Costa, C. M. Pereira, M. N. D. S. Cordeiro, *Phys. Chem. Chem. Phys.,* **18**, 2617 (2016).
62. P. R. Kumar, Y. H. Jung, C. H. Lim, D. K. Kim, *J. Mater. Chem. A,* **3**, 6271 (2015).
63. T. Broux, T. Bamine, F. Fauth, L. Simonelli, W. Olszewski, C. Marini, M. Menetrier, D. Carlier, C. Masquelier, L. Croguennec, *Chem. Mater.,* **28**, 7683 (2016).
64. M. Bianchini, F. Fauth, N. Brisset, F. Weill, E. Suard, C. Masquelier, L. Croguennec, *Chem. Mater.,* **27**, 3009 (2015).
65. Q. Liu, D. Wang, X. Yang, N. Chen, C. Wang, X. Bie, Y. Wei, G. Chen, F. Du, *J. Mater. Chem. A,* **3**, 21478 (2015).
66. Y. Cai, X. Cao, Z. Luo, G. Fang, F. Liu, J. Zhou, A. Pan, S. Liang, J. Zhou, A. Pan, S. Liang, *Adv. Sci.,* **5**, 1800680 (2018).
67. Y.-U. Park, D.-H. Seo, H. Kim, J. Kim, S. Lee, B. Kim, K. Kang, *Adv. Funct. Mater.,* **24**, 4603 (2014).